Microscopic theory of electric polarization induced by skyrmionic order in GaV₄S₈

S. A. Nikolaev[1,*] and I. V. Solovyev[1,2,†]

[1]*National Institute for Materials Science, MANA, 1-1 Namiki, Tsukuba, Ibaraki 305-0044, Japan*
[2]*Department of Theoretical Physics and Applied Mathematics, Ural Federal University, Mira Street 19, 620002 Yekaterinburg, Russia*

The lacunar spinel GaV₄S₈ was recently suggested to be a prototype multiferroic material hosting skyrmion lattice states with a sizable polarization $\boldsymbol{P}$ coupled to magnetic order. We explain this phenomenon on the microscopic level. On the basis of density functional theory, we construct an effective model describing the behavior of magnetically active electrons in a weakly coupled lattice formed by *molecular* orbitals of the $(V_4S_4)^{5+}$ clusters. By applying superexchange theory combined with the Berry-phase theory for $\boldsymbol{P}$, we derive a compass model relating the energy *and polarization* change with the directions of spins $\boldsymbol{e}_i$ in magnetic bonds. We argue that, although each skyrmion layer is mainly formed by superexchange interactions in the same plane, the spin dependence of $\boldsymbol{P}$ arises from the stacking misalignment of such planes in the perpendicular direction, which is inherent to the lacunar spinel structure. We predict a strong competition of isotropic, $\sim \boldsymbol{e}_i \boldsymbol{e}_j$, and antisymmetric, $\sim \boldsymbol{e}_i \times \boldsymbol{e}_j$, contributions to $\boldsymbol{P}$ that explains the experimentally observed effect.

DOI: 10.1103/PhysRevB.99.100401

Introduction. In recent years, magnetic skyrmions [1,2], topologically protected spin textures, have attracted high levels of interest due to their various potentials in the emerging field of spintronics [3]. In most cases, they are stabilized by Dzyaloshinskii-Moriya (DM) interactions in compounds with macroscopically broken inversion symmetry [4,5]. Owing to their topology and nanometer size, skyrmions behave as particle objects that can be moved over macroscopic distances by applying low-density electric currents [6,7] making them suitable candidates for applications in low-power nanoelectronics and data storage [8].

Skyrmionic states have been theoretically predicted to occur in crystals belonging to certain crystallographic classes, which can be either polar or nonpolar [1]. Being mostly observed in nonpolar chiral structures, skyrmions in polar crystals are also of great interest due to their interplay with electric polarization, giving rise to fascinating multiferroic properties. Until recently, Cu₂OSeO₃ was the only known multiferroic material hosting a skyrmionic state [9,10]. Shortly after its first observation, an electric field control of the skyrmion lattice in Cu₂OSeO₃ has been reported, indicating that many emergent properties of the skyrmion state can be tailored to the properties of a host material [11,12]. Overall, multiferroicity may give rise to many new prospects in a nondissipative electric field control of magnetic objects, and the existence of skyrmionic states in insulating magnetoelectric materials holds many potential applications for new-generation electronic devices.

Recently, a novel host material has been reported to exhibit these properties [13]. GaV₄S₈ is a member of the lacunar spinel family with a noncentrosymmetric nonpolar cubic $F\bar{4}3m$ structure, which at 38 K undergoes a structural transition to the polar rhombohedral $R3m$ phase [14], giving rise to the ferroelectric polarization $\sim$6000 μC/m² along the rhombohedral direction $z \parallel$ [111] [15]. A complex phase diagram comprising paramagnetic, ferromagnetic (FM), skyrmion, and cycloidal states has been demonstrated, where the spin-driven excess polarization was assigned in each magnetic phase with a total value of $\sim$100 μC/m², almost two orders of magnitude larger than that of Cu₂OSeO₃ [15].

The existence of multiple ferroelectric phases in GaV₄S₈ indicates a complex interplay of charge, spin, and lattice degrees of freedom, making their theoretical description extremely important. Nevertheless, a rigorous theory of magnetoelectric coupling in skyrmion materials is lacking. It remains largely unknown what mechanisms are responsible for this coupling, what aspects of the crystal structure play an essential role, and how a spin texture contributes to electric polarization in each ferroelectric phase. Thus, the purpose of this Rapid Communication is to fill this gap and explain the multiferroic properties of GaV₄S₈ on a microscopic level, through the rigorous Berry-phase theory of electric polarization combined with a realistic modeling approach.

Electronic model. According to electronic structure calculations within the local density approximation (LDA) [16], as implemented in the VASP [17] and QUANTUM ESPRESSO [18] packages, the group of bands near the Fermi level is dominated by the V 3d states [Fig. 1(a)], which strongly hybridize within each of the $(V_4S_4)^{5+}$ clusters, thus forming molecular-type orbitals. The hybridization between these molecular orbitals is considerably weak and leads to weakly dispersive bands. In the $F\bar{4}3m$ phase, the molecular states belong to the a_1', e', and t_2 representations and are filled with seven electrons. Thus, the low-lying a_1' and e' states are double occupied and do not contribute to magnetism, while the highest threefold degenerate t_2 level accommodates one unpaired electron. The rhombohedral distortion in the $R3m$

———————
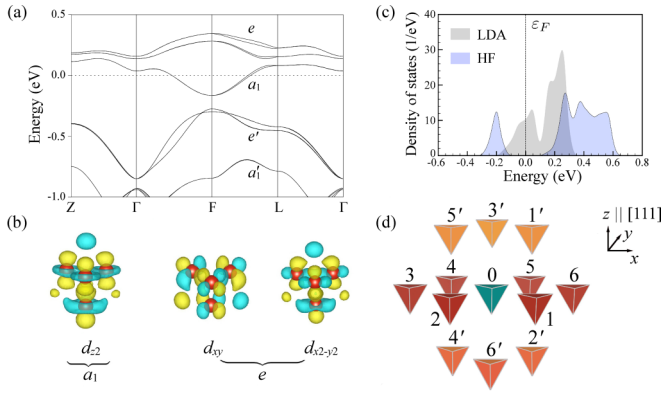*saishi@inbox.ru
†solovyev.igor@nims.go.jp

FIG. 1. (a) Bands located near the Fermi level as calculated within LDA including spin-orbit coupling for the low-temperature GaV_4S_8. (b) Wannier functions representing the high-lying a_1 and e states. (c) Density of states as obtained from LDA and Hartree-Fock calculations. (d) Schematic view of the V_4 clusters with nearest neighbors.

phase lifts the degeneracy of the t_2 level, splitting it into a single a_1 and twofold degenerate e states.

Carrying a local $S = \frac{1}{2}$ moment, the $(V_4S_4)^{5+}$ clusters can be regarded as magnetic building blocks, and the corresponding molecular $a_1 \oplus e$ orbitals associated with the lattice of the V_4 tetrahedra can be chosen as a proper basis for the low-energy electronic model. In this regard, conventional band-structure methods may fail to properly include the electronic correlations between these composite molecular orbitals. Moreover, the complexity of skyrmion lattices, including hundreds of magnetic sites, is beyond the current abilities of *ab initio* techniques, and a model Hamiltonian approach turns out to be an essential tool to study the magnetic properties of GaV_4S_8. Thus, our first goal is to construct an effective Hubbard-type model while taking full advantage of the *ab initio* calculations in the Wannier basis,

$$\hat{\mathcal{H}}^{el} = \hat{\mathcal{H}}_{kin} + \hat{\mathcal{H}}_{CF} + \hat{\mathcal{H}}_{SO} + \hat{\mathcal{H}}_U. \quad (1)$$

The kinetic energy, $\hat{\mathcal{H}}_{kin} = \sum_{i \neq j} \sum_{ab\sigma} t_{ij}^{ab} \hat{c}_{ia}^{\sigma\dagger} \hat{c}_{jb}^{\sigma}$, crystal-field splitting, $\hat{\mathcal{H}}_{CF} = \sum_{i,a \in e,\sigma} \Delta \hat{c}_{ia}^{\sigma\dagger} \hat{c}_{ia}^{\sigma}$, and spin-orbit coupling (SOC) terms are identified through the matrix elements of the LDA Hamiltonian in the basis of *molecular-type* Wannier orbitals [19,20]; $\hat{c}_{ia}^{\sigma\dagger}$ ($\hat{c}_{ia}^{\sigma}$) are the corresponding creation (annihilation) operators of an electron with spin σ at site i and orbital a [$a = 1$ stands for the $a_1 = d_{z^2}$ orbital, and $a = 2$ and 3 stand for, respectively, $e = d_{xy}$ and $d_{x^2-y^2}$ orbitals, carrying also some weight of the yz and zx symmetry [21], as shown in Fig. 1(b)].

The full set of model parameters is presented in the Supplemental Material [22]. The polar rhombohedral distortion gives rise to the crystal-field splitting, $\Delta = 98.1$ meV. The site-diagonal part of $\hat{\mathcal{H}}_{SO}$ includes a conventional "spherical" term and the Rashba-type (R) contribution arising from the distortion [23], $\hat{\mathcal{H}}_{SO} = \zeta_{SO} \sum_i \hat{L}_i \cdot \hat{S}_i - \zeta_{SO}^R \sum_i (\hat{L}_i^x \hat{S}_i^x + \hat{L}_i^y \hat{S}_i^y)$, where the angular momentum operator is given in a compact form in terms of the antisymmetric Levi-Civita symbol as $(\hat{L}_i^x)^{ab} = -i\varepsilon_{2ab}$, $(\hat{L}_i^y)^{ab} = -i\varepsilon_{3ab}$, and $(\hat{L}_i^z)^{ab} = i\varepsilon_{1ab}$, and

the calculated SOC constants are $\zeta_{SO} = 23.0$ meV and $\zeta_{SO}^R = 1.3$ meV. The theory of superexchange (SE) used below utilizes only those hopping parameters that involve the occupied a_1 orbital, $\vec{t}_{ij}^1 = (t_{ij}^{11}, t_{ij}^{12}, t_{ij}^{13})$. For the in-plane bonds [$j = 1$–6 in Fig. 1(d)] these parameters are given by $\vec{t}_{0j} = (-1)^j t_\parallel^S (0, \sin\frac{\pi j}{3}, \cos\frac{\pi j}{3}) + t_\parallel^A(\theta_\parallel, \cos\frac{\pi j}{3}, -\sin\frac{\pi j}{3})$, where $t_\parallel^S = -25$ meV and $t_\parallel^A = -16$ meV stand for symmetric and antisymmetric parts, respectively, and $\theta_\parallel = 0.25$. For the out-of-plane bonds [$j = 1'$–6' in Fig. 1(d)] we have $\vec{t}_{0j} = (-1)^j t_\perp^S(0, -\sin\frac{\pi j}{3}, \cos\frac{\pi j}{3}) + t_\perp^A(\theta_\perp, -\sin\frac{\pi j}{3}, \cos\frac{\pi j}{3})$, where $t_\perp^S = -23$ meV, $t_\perp^A = -22$ meV, and $\theta_\perp = 0.15$. Finally, the screened on-site Coulomb interactions,

$$\hat{\mathcal{H}}_U = \frac{1}{2} \sum_i \sum_{\sigma\sigma'} \sum_{abcd} U^{abcd} \hat{c}_{ia}^{\sigma\dagger} \hat{c}_{ic}^{\sigma'\dagger} \hat{c}_{ib}^{\sigma} \hat{c}_{id}^{\sigma'}, \quad (2)$$

were evaluated by using the constrained random phase approximation (cRPA) [24]. The calculated values are $U \equiv U_{nnnn} = 0.68$ eV and $J \equiv U_{nmmn} = 0.08$ eV for the intraorbital Coulomb and Hund's rule exchange interactions, respectively. These values are not particularly strong because the molecular t_2 orbitals are rather extended in space, considerably reducing the bare interactions compared to their regular atomic values. Furthermore, the bare interactions are efficiently screened in cRPA due to the proximity of the target t_2 bands to the occupied a_1' and e' bands of the same V $3d$ character [25]. Nevertheless, U remains the largest parameter of the model that justifies the use of SE theory for constructing the spin model in the limit $\hat{t}_{ij} \ll U$ [26].

The electronic model (1) can be solved in the mean-field Hartree-Fock approximation [25], and the FM state with the indirect band gap of 0.15 eV is found to be the ground state for the low-temperature phase of GaV_4S_8 [Fig. 1(c)]. Given the large hopping parameters between occupied a_1 and empty e states, the FM ground state is also favored by the Goodenough-Kanamori rule [27,28].

Spin model. In the atomic limit, a single t_2 electron resides at the lowest Kramers doublet of $\hat{\mathcal{H}}_{CF} + \hat{\mathcal{H}}_{SO}$, $|\alpha_i\rangle$, and the corresponding Wannier function at site i, $|w_i\rangle = |\alpha_i\rangle$, specifies the direction of spin as $\mathbf{e}_i = \langle\alpha_i|\boldsymbol{\sigma}|\alpha_i\rangle/|\langle\alpha_i|\boldsymbol{\sigma}|\alpha_i\rangle|$. The inclusion of $\hat{t}_{ij}$ will induce the tails $|\alpha_{i \to j}\rangle$ of $|w_i\rangle$ spreading to neighboring sites j,

$$|w_i\rangle \approx |\alpha_i\rangle + |\alpha_{i \to j}\rangle, \quad (3)$$

which can be evaluated within perturbation theory to first order in $\hat{t}_{ij}$ by considering virtual hoppings into the subspace of unoccupied states at the neighboring sites (and vice versa) as $|\alpha_{i \to j}\rangle = \hat{\mathcal{M}}_j \hat{t}_{ji} |\alpha_i\rangle$, where

$$\hat{\mathcal{M}}_j = \sum_M \frac{\hat{\mathcal{P}}_j |jM\rangle\langle jM|\hat{\mathcal{P}}_j}{E_{jM}},$$

E_{jM} and $|jM\rangle$ are, respectively, eigenvalues and eigenfunctions of the excited two-electron states at site j, constructed from $\hat{\mathcal{H}}_{CF} + \hat{\mathcal{H}}_{SO} + \hat{\mathcal{H}}_U$ in the basis of Slater determinants by using Slater-Condon rules, and $\hat{\mathcal{P}}_j$ is the projector operator in the form of two-electron Slater determinants, constructed from the occupied orbital $|\alpha_j\rangle$ and basis orbitals at site j (thus enforcing the Pauli principle) [29–31]. Then, the kinetic energy gain can be expressed as

$E_{\text{kin}} = \sum_{\langle ij \rangle} (\langle \alpha_i | \hat{t}_{ij} | \alpha_{i \to j} \rangle + i \leftrightarrow j)$. By considering all possible combinations of $|\alpha_i\rangle$ and $|\alpha_j\rangle$, corresponding to the x, y, and z directions of spins at sites i and j, E_{kin} can be mapped onto the spin model $\mathcal{H}^S = \sum_{\langle ij \rangle} \boldsymbol{e}_i \overset{\leftrightarrow}{\mathcal{J}}_{ij} \boldsymbol{e}_j$, which is further rearranged as [22]

$$\mathcal{H}^S = \sum_{\langle ij \rangle} (-J_{ij}\boldsymbol{e}_i\boldsymbol{e}_j + \boldsymbol{D}_{ij}\boldsymbol{e}_i \times \boldsymbol{e}_j + \boldsymbol{e}_i \overset{\leftrightarrow}{\Gamma}_{ij}\boldsymbol{e}_j), \quad (4)$$

in terms of the isotropic exchange constants J_{ij}, antisymmetric DM vectors $\boldsymbol{D}_{ij}$, and the traceless symmetric anisotropic tensors $\overset{\leftrightarrow}{\Gamma}_{ij}$. Using parameters of the electronic model (1), we obtain $J_\parallel = 0.180$ meV and $J_\perp = 0.217$ meV for the nearest-neighbor in-plane and out-of-plane interactions, respectively [$j = 1\text{–}6$ and $1'\text{–}6'$ in Fig. 1(d)]. The corresponding Curie temperature $T_C \sim 10$ K estimated in the random phase approximation [32] is close to the experimental value of 13 K. The resulting DM interactions can be written in compact form as $\boldsymbol{D}_{0j} = d_\parallel[\sin\frac{\pi j}{3}, \cos\frac{\pi j}{3}, (-1)^j\delta]$ for $j = 1\text{–}6$, where $d_\parallel = 0.073$ meV and $\delta = 0.137$, and $\boldsymbol{D}_{0j} = d_\perp(\cos\frac{\pi j}{3}, \sin\frac{\pi j}{3}, 0)$ for $j = 1'\text{–}6'$, where $d_\perp = 0.057$ meV. The parameters of $\overset{\leftrightarrow}{\Gamma}_{ij}$ can be neglected on account of their smallness [22].

Electric polarization. Such a theory of SE interactions is well established and constitutes the basis of the so-called anisotropic compass model, which is widely used for the analysis of magnetic properties of $5d$ iridium oxides [33]. In the following, we formulate a similar anisotropic compass model for electric polarization. The rigorous Berry-phase theory relates the polarization change with expectation values of the position operator, calculated in the Wannier functions basis for the occupied states [34],

$$\boldsymbol{P} = -\frac{e}{V} \sum_i^{\text{occ}} \langle w_i | \boldsymbol{r} | w_i \rangle, \quad (5)$$

where $-e$ and V is the electron charge and the unit cell volume, respectively. By this definition, all spin dependencies of $\boldsymbol{P}$ are incorporated in $|w_i\rangle$, so one needs to evaluate the change in the distribution of $|w_i\rangle$ caused by the change of magnetic order. In the lattice model, this change can be described by the tails of Wannier functions $|\alpha_{i \to j}\rangle$ spreading to neighboring sites. Then, substituting Eq. (3) in Eq. (5), electric polarization can be expressed as a sum of bond contributions $\boldsymbol{P} = \sum_{\langle ij \rangle} \boldsymbol{P}_{ij}$ [35], where

$$\boldsymbol{P}_{ij} = \frac{e}{V} \boldsymbol{\tau}_{ji} (\langle \alpha_{j \to i} | \alpha_{j \to i} \rangle - \langle \alpha_{i \to j} | \alpha_{i \to j} \rangle), \quad (6)$$

and $\boldsymbol{\tau}_{ji} = \boldsymbol{R}_j - \boldsymbol{R}_i$ is the bond vector connecting neighboring sites [36–38]. The quantity $\langle \alpha_{i \to j} | \alpha_{i \to j} \rangle$, which is merely the Wannier weight transfer from site i to site j, can be obtained in the framework of SE theory as $\langle \alpha_{i \to j} | \alpha_{i \to j} \rangle = \langle \alpha_i | \hat{t}_{ij} \hat{\mathcal{M}}_j^2 \hat{t}_{ji} | \alpha_i \rangle$. By considering different directions of spins for $|\alpha_i\rangle$ and $|\alpha_j\rangle$, the spin-driven part of electric polarization can be written as $\boldsymbol{P} = \sum_{\langle ij \rangle} \boldsymbol{\epsilon}_{ji}(\boldsymbol{e}_i \overset{\leftrightarrow}{\mathcal{P}}_{ij} \boldsymbol{e}_j)$ or

$$\boldsymbol{P} = \sum_{\langle ij \rangle} \boldsymbol{\epsilon}_{ji}(P_{ij}\boldsymbol{e}_i\boldsymbol{e}_j + \boldsymbol{\mathcal{P}}_{ij}\boldsymbol{e}_i \times \boldsymbol{e}_j + \boldsymbol{e}_i \overset{\leftrightarrow}{\Pi}_{ij}\boldsymbol{e}_j), \quad (7)$$

where $\boldsymbol{\epsilon}_{ji} = \boldsymbol{\tau}_{ji}/|\boldsymbol{\tau}_{ji}|$. This is an analog of Eq. (4), where $\boldsymbol{\epsilon}_{ji}P_{ij}$, $\boldsymbol{\epsilon}_{ji}\boldsymbol{\mathcal{P}}_{ij}$, and $\boldsymbol{\epsilon}_{ji}\overset{\leftrightarrow}{\Pi}_{ij}$ stand for isotropic, antisymmetric, and anisotropic symmetric contributions, respectively [39].

Importantly, since $\boldsymbol{P}_{ij} \parallel \boldsymbol{\epsilon}_{ji}$, *only the out-of-plane bonds can contribute to the polarization change along z.*

In order to clarify the microscopic origin of electric polarization in GaV$_4$S$_8$, it is useful to consider an analytical expression for P_{ij}, which can be easily obtained in the absence of SOC. To first order in $J/(U + \Delta)$, it yields [22] $P_{ij} \approx (e|\boldsymbol{\tau}_{ji}|/V)\mathcal{T}_{ij}J/(U + \Delta)^3$, where $\mathcal{T}_{ij} = (t_{ji}^{12})^2 + (t_{ji}^{13})^2 - (t_{ij}^{12})^2 - (t_{ij}^{13})^2$ is the antisymmetric tensor ($\mathcal{T}_{ij} = -\mathcal{T}_{ji}$). Thus, in order to have finite P_{ij}, it is essential that (i) the Hund's rule coupling J should be finite, and (ii) inversion symmetry of the bond connecting neighboring sites i and j should be crystallographically broken (otherwise, $\mathcal{T}_{ij} = \mathcal{T}_{ji}$ and, therefore, $\mathcal{T}_{ij} = 0$, as indeed happens in the high-temperature $F\bar{4}3m$ phase). These two properties hold even in the presence of SOC. Particularly, if $J = 0$, the entire tensor $\overset{\leftrightarrow}{\mathcal{P}}_{ij}$ is identically equal to zero, as confirmed by our calculations. Furthermore, for equivalent bonds in the positive ($+$) and negative ($-$) directions of z, we have $\mathcal{T}^- = -\mathcal{T}^+$, which is the direct consequence of translational invariance and the antisymmetry of $\mathcal{T}_{ij}$. In combination with $\boldsymbol{\epsilon}_{ji} = -\boldsymbol{\epsilon}_{ij}$, it results in a finite contribution to $\boldsymbol{P}$.

The calculated parameters for $j = 1'\text{–}6'$ are $P_{0j} = (-1)^j P_\perp$ and $\boldsymbol{\mathcal{P}}_{0j} = (-1)^j p_\perp(\cos\frac{\pi j}{3}, \sin\frac{\pi j}{3}, 0)$, where $P_\perp = -362$ μC/m^2 and $p_\perp = 41$ μC/m^2. As we will see below, they are mainly responsible for the magnetic state dependence of P^z. The corresponding polarization in the FM phase is calculated from Eq. (7) as $P^z = 3\epsilon_{01'}^z P_\perp = 889$ μC/m^2 (where $\epsilon_{01'}^z = 0.819$ [14]), while its thermal average in the paramagnetic state yields $P^z = 0$. As a result, we expect a large spin-driven excess polarization in the FM phase. The effect is very generic and can readily take place in other polar magnets [40,41]. For the in-plane bonds $j = 1\text{–}6$, we have $P_\parallel \equiv 0$ and $\boldsymbol{\mathcal{P}}_{0j} = (-1)^j p_\parallel(\cos\frac{\pi j}{3}, -\sin\frac{\pi j}{3}, 0)$, where $p_\parallel = 30$ μC/m^2. Since $\epsilon_{0j}^z = 0$, these bonds do not contribute to P^z. Nevertheless, $\boldsymbol{\mathcal{P}}_{0j}$ can give rise to small $P^{x,y}$, provided that the symmetry is lowered by magnetic order, as in the proper-screw spin spiral [36,42]. Finally, in the multidomain samples [13], the value of P^z will be deteriorated: In the domains [1$\bar{1}\bar{1}$], [$\bar{1}$1$\bar{1}$], and [$\bar{1}\bar{1}$1], $\boldsymbol{P}$ is parallel to the corresponding rhombohedral axes, whose z component is opposite to the one of the main domain [111]. Moreover, since $P_\parallel = 0$, there are no other contributions to P^z coming from the domains [1$\bar{1}\bar{1}$], [$\bar{1}$1$\bar{1}$], and [$\bar{1}\bar{1}$1]. This can explain a relatively small value of spin-driven polarization (~100 μC/m^2) observed experimentally [15], in comparison with the results of our theoretical calculations.

Phase diagram. We perform classical Monte Carlo calculations for the spin model (4) with an applied magnetic field $h \parallel z$ by using a heat-bath algorithm combined with overrelaxation [22,43]. In these calculations, we assume that DM interactions are mainly responsible for the in-plane non-collinear alignment of spins and neglect possible spatial modulations of the magnetic textures along z. This is consistent with experimental neutron scattering data [13] that report no magnetic superstructures along the direction of the magnetic field. The results calculated for supercells with the minimal periodicity along z are shown in Fig. 2(a) and nicely reproduce the main sequence of cycloidal→skyrmionic→FM states in the phase diagram of GaV$_4$S$_8$ with the increase of h [15].
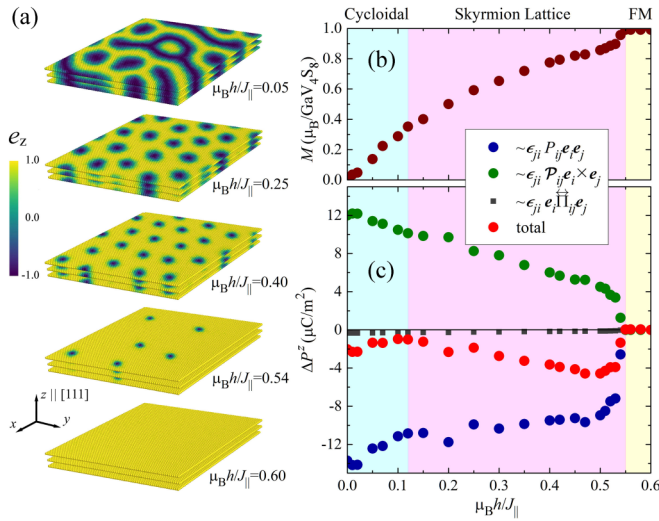
FIG. 2. (a) Spin patterns as obtained in Monte Carlo calculations for the model (4) with an applied magnetic field $h \parallel z$ at temperature $T = 0.1J_\parallel$ for the supercell of $72 \times 72 \times 3$ spins with periodic boundary conditions. In these notations, a "skyrmion lattice" means the lattice of well-distinguished skyrmionic tubes of the same size, while a "cycloidal phase" includes large interconnected regions with the same direction of spins. The corresponding h dependence of (b) the magnetization and (c) electric polarization: total and partial contributions, calculated from Eq. (7) relative to the FM state.

As seen, the two-dimensional spin patterns tend to stack ferromagnetically along z, that is naturally explained by $J_\perp$. In the GaV$_4$S$_8$ structure, this stacking of monolayers is misaligned by the rhombohedral translations, so that the adjacent skyrmionic layers experience an additional shift in the xy plane. Therefore, there will always be some noncollinearity of spins between the adjacent layers [44] that, according to Eq. (7), will contribute to the excess spin-driven polarization.

In order to describe this effect quantitatively, we evaluate the total and partial contributions to P^z by using Eq. (7) and the distribution of spins $\{e_i\}$ obtained in Monte Carlo calculations. The results are summarized in Fig. 2(c), where we use the FM state as the reference point. Particularly, we note a strong competition of the isotropic ($\sim e_i e_j$) and antisymmetric ($\sim e_i \times e_j$) contributions, while the anisotropic

symmetric part ($\sim e_i \overset{\leftrightarrow}{\Pi}_{ij} e_j$) is negligibly small. As expected, the antisymmetric contribution decreases with the increase of h and vanishes in the collinear FM state. On the contrary, the isotropic contribution takes its maximal value in the FM state and is further reduced by a noncollinear alignment of spins. Since the change of $e_i \times e_j$ and $e_i e_j$ is proportional to ϕ_{ij} and ϕ_{ij}^2, respectively (with ϕ_{ij} being the angle between e_i and e_j, which is induced by DM interactions and proportional to ζ_{SO}), both the isotropic and antisymmetric mechanisms are of second order in ζ_{SO}, while the change of $e_i \overset{\leftrightarrow}{\Pi}_{ij} e_j$ is only of third order. This naturally explains the hierarchy of partial contributions to ΔP^z in Fig. 2(c). Furthermore, the antisymmetric mechanism dominates when the skyrmions are large and the spin texture slowly varies in space. In this region, electric polarization decreases with h, in agreement with the experimental observation [15]. The corresponding polarization change of about 4 μC/m^2 is also consistent with experimental data [15]. Finally, our conclusion clearly differs from the phenomenological analysis presented in Ref. [15], arguing that the antisymmetric DM interactions are solely needed to stabilize the cycloidal and skyrmion phases, while the corresponding polarization change is driven by the isotropic and anisotropic symmetric terms. In fact, we also expect a small region in the phase diagram, where the magnetization is nearly saturated [Fig. 2(b)] and the skyrmion size is small, so the polarization change is mainly governed by the isotropic mechanism and is expected to increase with h. Overall, the h dependence of spin-driven polarization in the skyrmion phase depends on the skyrmion size and the way a skyrmion lattice is packed, leading to different competing scenarios. Finally, it is worth noting that spin structure modulations driven by the out-of-plane DM interactions may also take place and increase the antisymmetric contribution to spin-driven polarization.

Conclusion. We have presented the microscopic theory of spin-driven electric polarization in GaV$_4$S$_8$. Based on the realistic model derived from first-principles electronic structure calculations, we have shown that the spin-excess polarization along the rhombohedral z axis associated with the ferromagnetic, skyrmionic, and cycloidal states, is given by the *interlayer* electron transfer and originates from the strongly competing isotropic and antisymmetric contributions. The proposed theory is very general and can be applied to other multiferroic materials, including those hosting skyrmionic states.

[1] A. N. Bogdanov and D. A. Yablonskii, Sov. Phys. JETP **68**, 101 (1989).

[2] U. K. Rößler, A. N. Bogdanov, and C. Pfleiderer, Nature (London) **442**, 797 (2006).

[3] N. Nagaosa and Y. Tokura, Nat. Nanotechnol. **8**, 899 (2013).

[4] S. Mühlbauer, B. Binz, F. Jonietz, C. Pfleiderer, A. Rosch, A. Neubauer, R. Georgii, and P. Böni, Science **323**, 915 (2009).

[5] X. Z. Yu, Y. Onose, N. Kanazawa, J. H. Park, J. H. Han, Y. Matsui, N. Nagaosa, and Y. Tokura, Nature (London) **465**, 901 (2010).

[6] T. Schulz, R. Ritz, A. Bauer, M. Halder, M. Wagner, C. Franz, C. Pfleiderer, K. Everschor, M. Garst, and A. Rosch, Nat. Phys. **8**, 301 (2012).

[7] X. Z. Yu, N. Kanazawa, W. Z. Zhang, T. Nagai, T. Hara, K. Kimoto, Y. Matsui, Y. Onose, and Y. Tokura, Nat. Commun. **3**, 988 (2012).

[8] A. Fert, V. Cros, and J. Sampaio, Nat. Nanotechnol. **8**, 152 (2013).

[9] S. Seki, X. Z. Yu, S. Ishiwata, and Y. Tokura, Science **336**, 198 (2012).

[10] T. Adams, A. Chacon, M. Wagner, A. Bauer, G. Brandl, B. Pedersen, H. Berger, P. Lemmens, and C. Pfleiderer, Phys. Rev. Lett. **108**, 237204 (2012).

[11] J. S. White, I. Levatić, A. A. Omrani, N. Egetenmeyer, K. Prša, I. Živković, J. L. Gavilano, J. Kohlbrecher, M. Bartkowiak, H. Berger, and H. M. Rønnow, J. Phys.: Condens. Matter **24**, 432201 (2012).

[12] J. S. White, K. Prša, P. Huang, A. A. Omrani, I. Živković, M. Bartkowiak, H. Berger, A. Magrez, J. L. Gavilano, G. Nagy, J. Zang, and H. M. Rønnow, Phys. Rev. Lett. **113**, 107203 (2014).

[13] I. Kézsmárki, S. Bordács, P. Milde, E. Neuber, L. M. Eng, J. S. White, H. M. Rønnow, C. D. Dewhurst, M. Mochizuki, K. Yanai, H. Nakamura, D. Ehlers, V. Tsurkan, and A. Loidl, Nat. Mater. **14**, 1116 (2015).

[14] R. Pocha, D. Johrendt, and R. Pottgen, Chem. Mater. **12**, 2882 (2000).

[15] E. Ruff, S. Widmann, P. Lunkenheimer, V. Tsurkan, S. Bordács, I. Kézsmárki, and A. Loidl, Sci. Adv. **10**, e1500916 (2015).

[16] W. Kohn and L. J. Sham, Phys. Rev. **140**, A1133 (1965).

[17] G. Kresse and J. Hafner, Phys. Rev. B **47**, 558 (1993).

[18] P. Giannozzi, S. Baroni, N. Bonini *et al.*, J. Phys.: Condens. Matter **21**, 395502 (2009).

[19] N. Marzari, A. A. Mostofi, J. R. Yates, I. Souza, and D. Vanderbilt, Rev. Mod. Phys. **84**, 1419 (2012).

[20] A. A. Mostofi, J. R. Yates, G. Pizzi, Y. S. Lee, I. Souza, D. Vanderbilt, and N. Marzari, Comput. Phys. Commun. **185**, 2309 (2014).

[21] K. Terakura, T. Oguchi, A. R. Williams, and J. Kübler, Phys. Rev. B **30**, 4734 (1984).

[22] See Supplemental Material at http://link.aps.org/supplemental/10.1103/PhysRevB.99.100401 for the full set of model parameters and calculation details, which includes Refs. [45–55].

[23] E. I. Rashba and V. I. Sheka, Fiz. Tverd. Tela **1**, 162 (1959) (in Russian) [English translation: Supplemental Material to the paper by G. Bihlmayer, O. Rader, and R. Winkler, Focus on the Rashba effect, New J. Phys. **17**, 050202 (2015)].

[24] F. Aryasetiawan, M. Imada, A. Georges, G. Kotliar, S. Biermann, and A. I. Lichtenstein, Phys. Rev. B **70**, 195104 (2004).

[25] I. V. Solovyev, J. Phys.: Condens. Matter **20**, 293201 (2008).

[26] P. W. Anderson, Phys. Rev. **115**, 2 (1959).

[27] J. Kanamori, Prog. Theor. Phys. **17**, 177 (1957).

[28] J. B. Goodenough, J. Phys. Chem. Solids **6**, 287 (1958).

[29] I. V. Solovyev, Phys. Rev. B **74**, 054412 (2006).

[30] I. V. Solovyev, New J. Phys. **11**, 093003 (2009).

[31] N. B. Perkins, Y. Sizyuk, and P. Wölfle, Phys. Rev. B **89**, 035143 (2014).

[32] S. V. Tyablikov, *Methods of Quantum Theory of Magnetism* (Nauka, Moscow, 1975).

[33] G. Jackeli and G. Khaliullin, Phys. Rev. Lett. **102**, 017205 (2009).

[34] R. Resta, Rev. Mod. Phys. **66**, 899 (1994).

[35] The on-site contribution $\langle \alpha_i | \mathbf{r} | \alpha_i \rangle$ to the polarization change was found to be small [22].

[36] I. V. Solovyev, Phys. Rev. B **95**, 214406 (2017).

[37] I. V. Solovyev and S. A. Nikolaev, Phys. Rev. B **87**, 144424 (2013).

[38] I. V. Solovyev and S. A. Nikolaev, Phys. Rev. B **90**, 184425 (2014).

[39] Note, however, because of the additional prefactor ϵ_{ji}, P_{ij} and $\overset{\leftrightarrow}{\Pi}_{ij}$ are *antisymmetric* with respect to the interchange of i and j, while $\mathcal{P}_{ij}$ is *symmetric*.

[40] T. Kurumaji, S. Ishiwata, and Y. Tokura, Phys. Rev. X **5**, 031034 (2015).

[41] Y. Wang, G. L. Pascut, B. Gao, T. A. Tyson, K. Haule, V. Kiryukhin, and S.-W. Cheong, Sci. Rep. **5**, 12268 (2015).

[42] T. Kurumaji, S. Seki, S. Ishiwata, H. Murakawa, Y. Tokunaga, Y. Kaneko, and Y. Tokura, Phys. Rev. Lett. **106**, 167206 (2011).

[43] D. P. Landau and K. Binder, *A Guide to Monte Carlo Simulations in Statistical Physics* (Cambridge University Press, Cambridge, UK, 2005).

[44] For example, if the skyrmion center is translated along the bond 0-1′ [Fig. 1(d)], the neighboring out-of-plane spins will stay noncollinear in two other bonds 0-3′ and 0-5′. These interlayer translations may take place randomly.

[45] K. Momma and F. Izumi, J. Appl. Crystallogr. **44**, 1272 (2011).

[46] P. E. Blochl, Phys. Rev. B **50**, 17953 (1994).

[47] H. J. Monkhorst and J. D. Pack, Phys. Rev. B **13**, 5188 (1976).

[48] M. Springer and F. Aryasetiawan, Phys. Rev. B **57**, 4364 (1998).

[49] J. Kanamori, Prog. Theor. Phys. **30**, 275 (1963).

[50] B. Drittler, M. Weinert, R. Zeller, and P. H. Dederichs, Phys. Rev. B **39**, 930 (1989).

[51] I. V. Solovyev, Phys. Rev. B **90**, 024417 (2014).

[52] K. I. Kugel and D. I. Khomskii, Sov. Phys. Usp. **25**, 231 (1982).

[53] A. M. Olés, G. Khaliullin, P. Horsch, and L. F. Feiner, Phys. Rev. B **72**, 214431 (2005).

[54] D. Vanderbilt and R. D. King-Smith, Phys. Rev. B **48**, 4442 (1993).

[55] I. V. Solovyev, Phys. Rev. B **91**, 224423 (2015).